Hindawi
Shock and Vibration
Volume 2018, Article ID 8142371, 12 pages
https://doi.org/10.1155/2018/8142371

Research Article

Online Structural Health Monitoring of Rotating Machinery via Ultrasonic Guided Waves

Ming Li,[1,2] **Guang Meng**,[2,3] **Hongguang Li**,[2] **Jianxi Qiu**,[2] **and Fucai Li**[2]

[1]*Shanghai Key Laboratory of Spacecraft Mechanism, Aerospace System Engineering Shanghai, Shanghai, China*
[2]*State Key Laboratory of Mechanical System and Vibration, Shanghai Jiao Tong University, Shanghai, China*
[3]*Shanghai Academy of Spaceflight Technology, Shanghai, China*

Correspondence should be addressed to Guang Meng; gmeng@sjtu.edu.cn

Received 3 February 2018; Revised 25 April 2018; Accepted 9 May 2018; Published 13 June 2018

Academic Editor: Marco Alfano

This paper focuses on the establishment of the online structural health monitoring strategy for rotating shafts using ultrasonic guided waves. The dispersion of cylindrical shaft is investigated and a conclusion that the longitudinal ultrasonic wave propagating along the cylindrical shaft can hardly be interfered by the rotation is obtained. The experimental system and the numerical simulation model have been constructed, based on the fact that the experimental research and the numerical verification have been conducted intensively. The strategy can be concluded no matter the cracked rotor is at rest or rotating. Comparing with the same rotor without crack, the amplitudes of the guided wave packages descend along the transmission path and the symmetric path where crack exists; however, the amplitude of the wave packages will ascend along the other transmission paths.

1. Introduction

As the most common fault in rotating machineries, crack should be cautiously monitored and treated. The crack fault always occurs under bad working conditions and propagates due to the alternative external loads. Ishida [1] reviewed the cases of crack faults in the industrial rotating machineries. It can be concluded from the history cases that the cracked rotor system cannot be diagnosed until the crack has propagated deeply enough, at least 25% of the diameter. If the diagnoses were not performed timely and properly, tragic accidents may happen. The most widely used crack diagnosis method is to arrange vibration sensors, usually eddy current sensors to monitor the radial vibration of the rotor. A previous research by the authors [2] interpreted the reason why the initial crack fault cannot be discovered when it has a relatively limited length and depth using Dynamic Saint-Venant Principle (DSVP). Therefore, it is necessary for the engineers and researchers to adopt other methods for monitoring the crack at the very early stage of propagation. Ultrasonic guided waves or elastic waves may be a better selection.

Ultrasonic guided wave has been extensively utilized in the structural health monitoring (SHM) and nondestructive testing and evaluation (NDT&E) of different stationary structures. Ditri [3] detected the circumferentially cracks in hollow cylinders using ultrasonic waves. Zhu et al. [4] simulated the nondestructive evaluation of hidden corrosion with ultrasonic waves using Boundary Element Method, and an experimental verification was also conducted. Lowe et al. [5] detected the defects in the pipe using ultrasonic wave and presented the relationship between the defect size and the strength of wave reflection. Qu et al. [6] implemented defect detection with ultrasonic wave on thick annular components. Tuzzeo and Lanza di Scalea [7] demonstrated the noncontact detection of the hidden corrosion defects in thin aluminum plates using micromachined gas(air)-coupled capacitive transducers. Lanza di Scalea et al. [8] carried out the defect detection of steel strands under three conditions, indentation in one of the helical wires away from the anchorages, indentations in two of the helical wires in the anchored region, and a cut for the entire cross section of a helical wire away from the anchorages using ultrasonic waves. Barshinge and Rose [9] researched the propagation characteristics of

ultrasonic waves in the elastic hollow cylinder coated with a viscoelastic material. Bartoli et al. [10] simulated a long-range damage detection of railroad tracks using Lamb wave. Li et al. [11] actuated Lamb wave in composite laminates using piezoelectric transducer and collected the signal by different fiber optic sensors in order to evaluate the defects. Moreover, the piezoelectric transducers array plays a vital role in the SHM and NDT&E using ultrasonic guided waves. Song et al. [12] studied the propagation of the ultrasonic waves actuated by piezoelectric transducers array in the honeycomb sandwich structures. Miao et al. [13] implemented the identification of dual notches in an aluminum plate based on piezoelectric transducers array, and a time-reverse algorithm was proposed. Li et al. [14] carried out an experimental study using piezoelectric transducers array on the ultrasonic wave propagation in the pressure vessel, and the results were compared with Finite Element simulation. A conclusion was pointed out that the L(0,2) mode is not sensitive to the contained liquid during its propagation, which is the most appropriate selection for damage detection for the pressure vessel.

In the retrieved papers on online damage detection of rotating shafts using ultrasonic wave, Han et al. [15] shot a projectile through an air gun to generate a longitudinal square stress wave in a cracked rotating shaft and then extracted the signal via noncontact magnetostrictive sensors. Wavelet transform was employed to process the wave signal to identify and locate the crack in the rotating shaft. Cho et al. [16] set up an experimental system using oblique magnetostrictive strips and carried out a noncontact generation, measurement, and application of torsional waves in damage detection of a rotating shaft. However, in their experiment, the circumferential crack in the rotating shaft is large and artificial, which shows an evident disparity with the practical fatigue cracks. Kim and Kim [17] applied Terfenol-D as the generators and transducers of stress wave on the damage detection of rotating shafts. Wang et al. [18] presented a method to detect crack on rotating shafts with longitudinal ultrasonic guided waves using Galfenol transducers. However, the authors only gave the simulation of experimental results, without implementing the experiment.

From the state-of-the-art review, two summings-up can be concluded. Firstly, the advantages on the SHM using ultrasonic guided waves on static structures such as hollow cylinders and thin plates have been demonstrated. The feasibilities of SHM on motional structures are potential, which would also be an important extension on ultrasonic guided waves. Secondly, the engineering level of the SHM system should be improved, including the method for guided wave generation and collection and the signal transmission. An advanced engineering level may lead to higher application feasibility in industrial field.

Based on the practical demands and the literature research, a system and method should be established in order to realize the online SHM for the rotating machineries. In the forthcoming sections, the dispersion of a cylindrical shaft is firstly discussed, then the experimental system and numerical simulation model are summarized. Finally, the propagation of ultrasonic guided waves and the damage detection via ultrasonic guided waves are elaborated based on foregoing research.

2. Dispersion of Cylindrical Shaft

Auriault [19] studied the dispersion of a rotating elastic medium and pointed out that the dilatational and shear waves are shown to be directly related to the Kibel number. Sharma and Grover [20] focused on the rotating thermoelastic media and a conclusion was made that there exist three kinds of waves, quasi-longitudinal wave, quasi-transverse wave, and thermal wave. However, a previous research by the authors [2] indicated that the elastic wave dispersion of the rotating cylindrical medium remains the same with the nonrotating cylindrical medium. Therefore, the dispersion of a cylindrical shaft should be foremost investigated.

There exists three modes in cylindrical medium of elastic waves, the longitudinal mode L(0,m), the torsional mode T(0,m), and the flexural mode F(n,m). The modes are derived from Pochhammer equation, which can be deduced from the displacement equations of the elastic waves propagating along the cylindrical shaft [2]. Suppose the cylindrical shaft has a radius a, and the velocities of the longitudinal wave and the transverse wave are c_L and c_T, respectively. Assume that the elastic wave has a circular frequency ω and a wave number κ, then

$$\begin{aligned} \alpha &= pa, \\ \beta &= qa, \\ \gamma &= \kappa a \end{aligned} \tag{1}$$

where $p^2 = \omega^2/c_L^2 - \kappa^2$, $q^2 = \omega^2/c_T^2 - \kappa^2$. Define

$$\Gamma_x = \frac{xJ_0(x)}{J_1(x)} \tag{2}$$

where J_0 and J_1 are Bessel functions. Then it can be deduced that the longitudinal mode satisfies [21]

$$2\alpha^2\left(\beta^2+\gamma^2\right) - \left(\beta^2-\gamma^2\right)^2\Gamma_\alpha - 4\alpha^2\gamma^2\Gamma_\beta = 0 \tag{3}$$

The torsional mode has the expression of [22]

$$\Gamma_\beta = 2 \tag{4}$$

and the roots

$$\begin{aligned} \beta_1 &= 0, \\ \beta_2 &= 5.136, \\ \beta_3 &= 8.417, \\ \beta_4 &= 11.62\ldots \end{aligned} \tag{5}$$

The flexural mode can be calculated using [23, 24]

$$J_1(\alpha)\,J_1^2(\beta)\left[u_1\Gamma_\beta^2 + u_2\Gamma_\alpha\Gamma_\beta + u_3\Gamma_\beta + u_4\Gamma_\alpha + u_5\right] = 0 \tag{6}$$

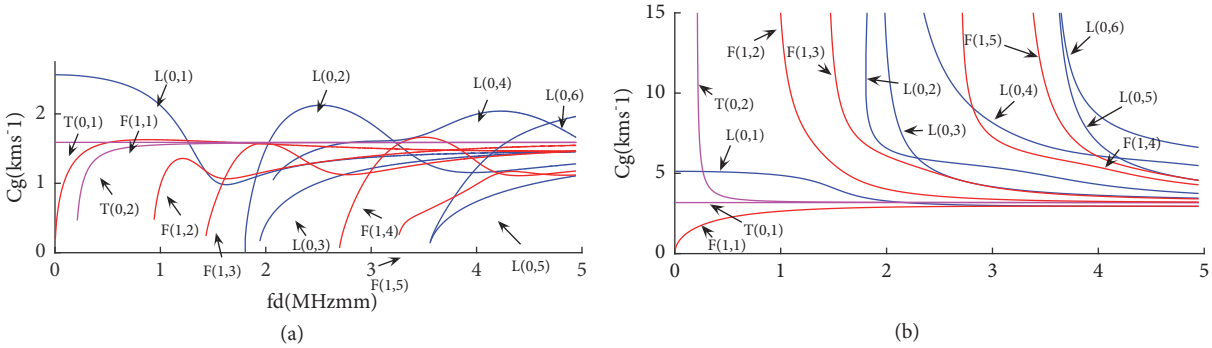

Figure 1: Dispersion curves of (a) phase velocity and (b) group velocity of a cylindrical shaft.

Herein,

$$u_1 = 2\left(\beta^2 - \gamma^2\right)^2$$
$$u_2 = 2\beta^2\left(5\gamma^2 + \beta^2\right)$$
$$u_3 = \beta^6 - 10\beta^4 - 2\beta^4\gamma^2 + 2\beta^2\gamma^2 + \beta^2\gamma^4 - 4\gamma^4 \quad (7)$$
$$u_4 = 2\beta^2\left(2\beta^2\gamma^2 - \beta^2 - 9\gamma^2\right)$$
$$u_5 = \beta^2\left(-\beta^4 + 8\beta^2 - 2\beta^2\gamma^2 + 8\gamma^2 - \gamma^4\right)$$

During the SHM using ultrasonic wave, the phase velocity $c_p = \omega/\kappa$ and group velocity $c_g = d\omega/d\kappa$ play very important roles. The relationship between c_p and c_g can be expressed as

$$c_g = \frac{c_p^2}{c_p - (fd)\left(\partial c_p/\partial\left(fd\right)\right)} \quad (8)$$

where $fd = 2fa$. Figure 1 illustrates the dispersion curves of (a) phase velocity and (b) group velocity, where the blue lines, the purple lines, and the red lines stand for the longitudinal mode L(0,m), the torsional mode T(0,m), and the flexural mode F(1,m), respectively.

It should be noted that, during the SHM, the excited modes, especially the longitudinal modes which carries majority of the energy, should be as few as possible in order to avoid the overlapping between wave packets. Furthermore, the group velocities of the excited modes should be separated in order to avoid the overlapping. Considering the criterions, $fa = 4.5MHzmm$ is optimal choice. Under this condition, L(0,4) and L(0,6) would be excited, which have faster velocities than other modes, and it is appropriate for wave packets identification without overlapping.

3. Experimental System and Numerical Simulation

3.1. Initial Crack. In the previous research of the authors [2], the definition has been proposed that initial crack is the crack at the very early stage of the propagation, which has limited length and depth and does not produce great variations on the stiffness of the rotor system. A crack belongs to initial crack when the influence on the stiffness of the rotor system it brings is less than 2%. It can also be deduced that when a crack belongs to initial crack, the ratio between the depth of crack and the diameter of the rotor $\overline{h}$ is less than 0.0215. In this research, $\overline{h} = 0.02$ is selected for the simulation and experiments.

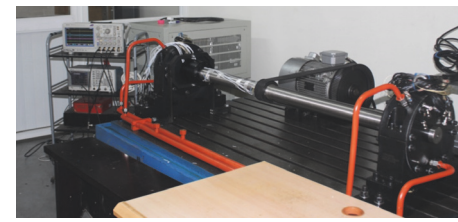

Figure 2: Overview of rotor structural health monitoring experimental system.

3.2. Experimental System. This experimental system was revamped from the turbo-expander experimental system in paper [25], which is illustrated in Figure 2. In this experiment, a rotor supported by two tilting pad bearings and driven by a synchronous belt is utilized, which has a diameter of 66mm.

Four pieces of 25×5mm piezoelectric transducers for guided waves excitation and four pieces for guided waves collection are arranged and numbered axial symmetrically around the rotor respectively, as illustrated in Figure 3. The distance between the excitation transducers and the collection transducers is 400mm. There are several advantages of the axial symmetrical arrangement. Firstly, a simultaneously excitation lead to an integral rather than local guided waves. Secondly, the axial symmetrical arrangement can eliminate the torsional and flexural modes to an extent. Finally, the collected signals can be compared spatiotemporally, which is appropriate for crack detection.

Figure 4 illustrates the slip ring and the manufactured crack. Due to the rotation of the rotor, a slip ring should be adopted in order to transmit the electrical signals between the transducers and the devices, such as the function generator, the amplifier, and the oscilloscope. It should be note that the manufactured crack is on the transmission path between no. 2 excitation transducer and no. 2 collection transducer. For

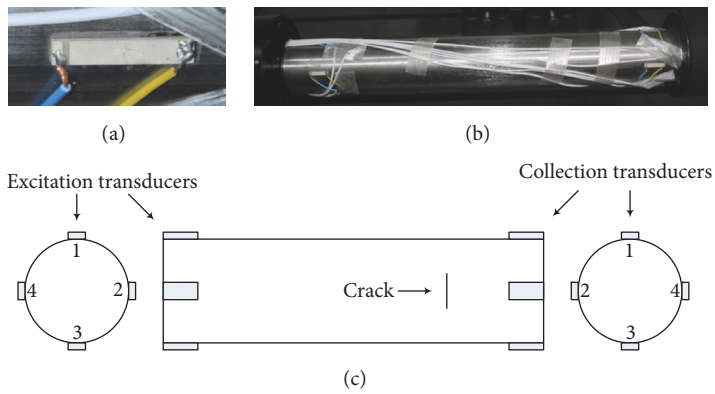

Figure 3: (a) Piezoelectric transducer, (b) photo of the arrangement of piezoelectric transducers array, and (c) sketch map of the arrangement of piezoelectric transducers array.

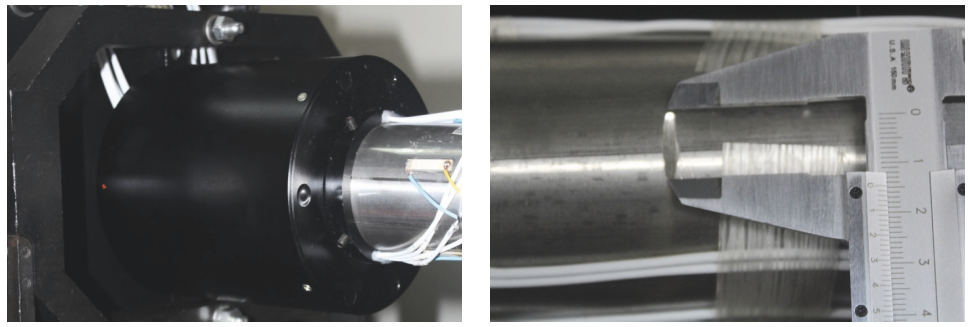

Figure 4: (a) Slip ring and (b) crack.

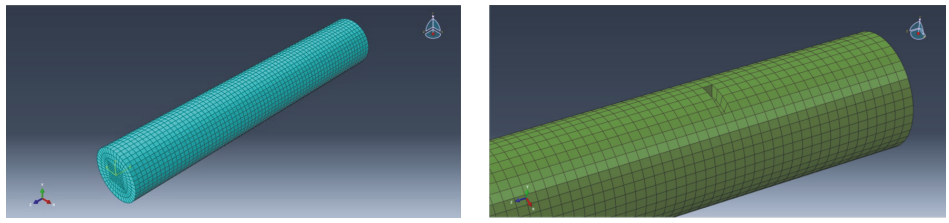

Figure 5: (a) FEM model of rotor and (b) FEM model with crack simulated by deleting elements.

the convenience, the transmission path between excitation transducer and collection transducer is named transmission path. Therefore, the crack is on the 2nd transmission path.

3.3. Numerical Simulation. The experimental results should be verified via numerical simulations. In the research of ultrasonic guided waves, Finite Element Method (FEM) [26] and Spectral Element Method (SEM) [27] have been widely adopted and proven in the previous investigations. Therefore, the results of numerical simulation can be a proper validation of the experimental results. In this research, FEM and the corresponding commercial software Abaqus are selected. Figure 5 illustrates the FEM model of the rotor without crack and the cracked rotor simulated by deleting elements.

4. Ultrasonic Wave Propagating along Rotating Shaft

4.1. Experimental Research. Figure 6 illustrates the input excitation signal to the function generator during the experiment, which is a Gaussian windowed 5-period sine signal with a 138kHz center frequency. Under this excitation, the longitudinal modes L(0,4) and L(0,6) are excited and the group velocity can be obtained from Figure 1(b), approximately 4.0km/s and 3.5km/s, respectively.

Moreover, the transmission waves collected by the piezoelectric transducers should be processed in order to suppress the disturbances. The electromagnetic interference is eliminated by 256 times average at the oscillation scope. The

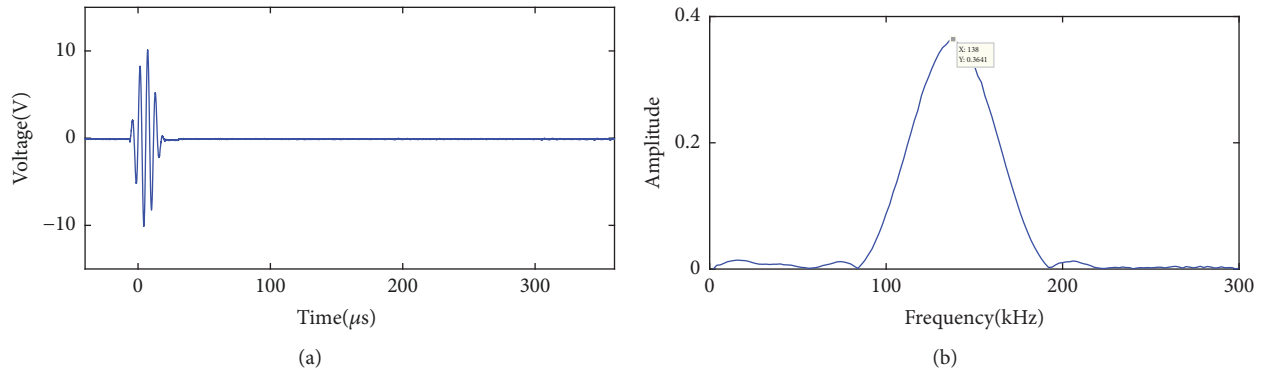

Figure 6: (a) Time-domain and (b) frequency-domain excitation signal of experiment.

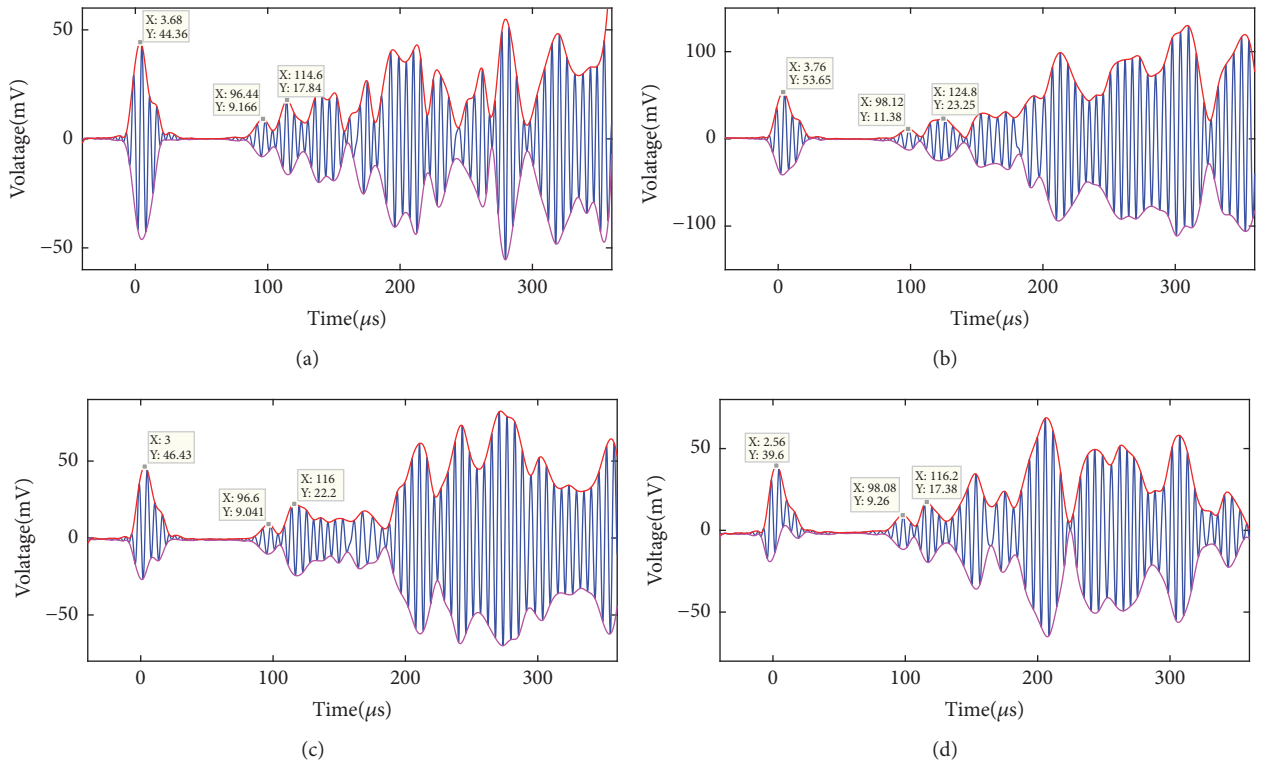

Figure 7: Collected signals of piezoelectric transducers after filtering (a) no. 1, (b) no. 2, (c) no. 3, and (d) no. 4 when the rotor is at rest.

time-shift is eliminated after utilizing a low-pass filter on the averaged signal. Finally, the upper and lower envelops are extracted for the following investigations. In this processing, the low-pass filter is designed by pulse-response method, and the pass-band and stop-band cut-off frequencies are set as 170kHz and 200kHz, respectively. The experiments are implemented when the rotor is at rest, and with a rotating speed of 900rpm, respectively, due to the limited speed of the slip ring.

4.1.1. Static Research. The processed ultrasonic guided wave signals collected by the piezoelectric transducers are illustrated in Figure 7. The first and second wave packages can be obviously identified, which are L(0,4) and L(0,6), respectively. The transmission time can be obtained from the figure, and the distance between the excitation transducers and collection transducers is given. Therefore, the average group velocity of L(0,4) and L(0,6) can be calculated, which are 4.25km/s and 3.49km/s, respectively. The group velocities calculated theoretically and experimentally coincide with each other considering the errors.

4.1.2. Dynamic Research. When the rotor rotates at 900rpm, i.e., 15Hz, the processed ultrasonic guided wave signals collected by the piezoelectric transducers are illustrated in Figure 8. It can be observed that the collected signals when the rotor rotates at 15Hz remain approximately the same with the collected signals when the rotor is at rest. The first and

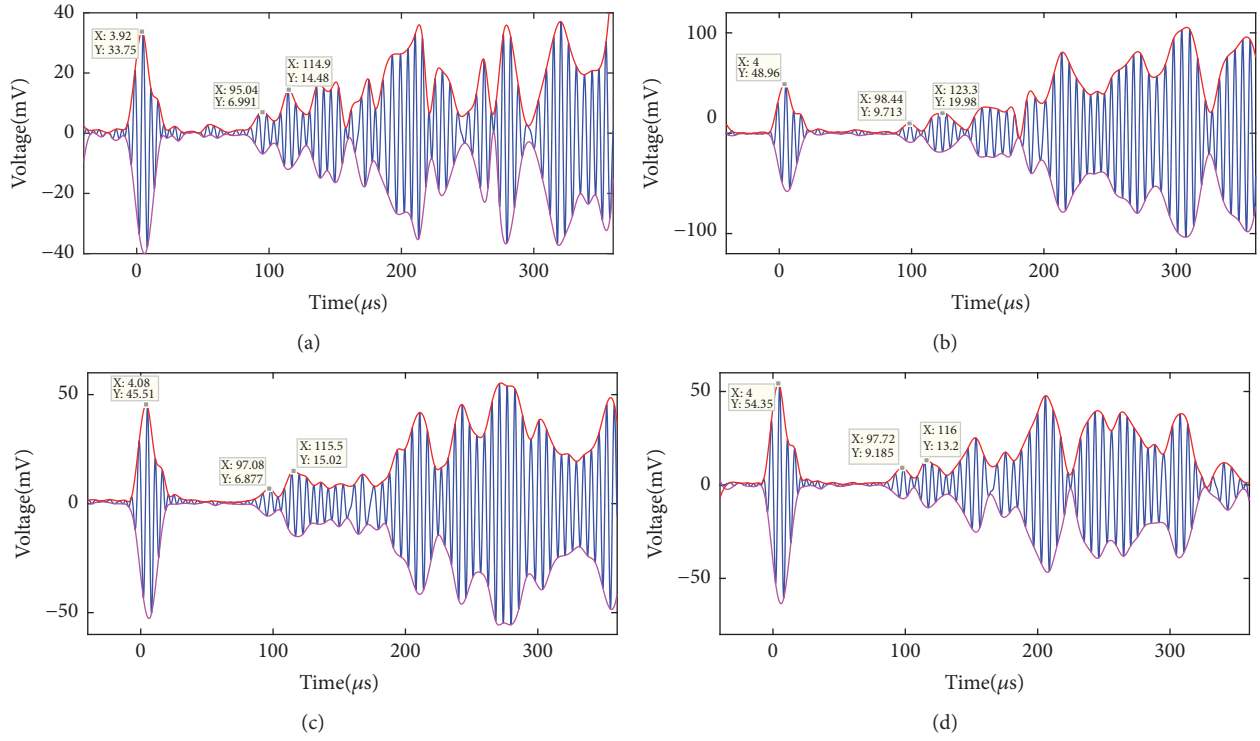

Figure 8: Collected signals of piezoelectric transducers after filtering (a) no. 1, (b) no. 2, (c) no. 3, and (d) no. 4 when the rotor rotates at 15Hz.

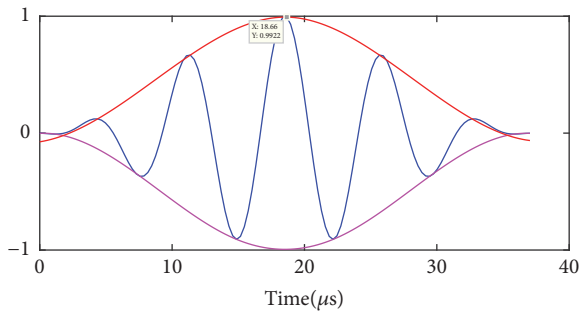

Figure 9: Excitation signal of FEM simulation.

the second wave packages can be obviously identified as well. The calculated group velocities are 4.30km/m and 3.53km/s, which indicates that the first and the second wave packages are still L(0,4) and L(0,6), respectively, considering the errors.

From the above studies it can be concluded that, in accordance with the DSVP analysis in paper [2], the longitudinal ultrasonic guided waves propagating along the cylindrical shaft can hardly be interfered by the rotation. Therefore, it is feasible to utilize L(0,4) and L(0,6) for the SHM of the rotor both at rest or rotating.

4.2. Numerical Verification. However, the experimental results should be verified by numerical simulations. The excitation procedure by the piezoelectric transducers is simulated by the surface tractions in FEM. The normalization excitation signal is illustrated in Figure 9, which is a Gaussian windowed 5-period sine signal with a 138kHz center frequency. The amplitude of stress per unit area is set to be 1MPa and the stress of the elements corresponding to the collection transducers is extracted to represent the voltage signals for the following numerical verification.

4.2.1. Static Verification. When the rotor is at rest, the stress signals collected at the corresponding elements via FEM simulation are illustrated in Figure 10. It can be observed that the signals obtained experimentally and numerically coincide with each other. The first and second wave packages can be clearly identified, which manifest L(0,4) and L(0,6). The calculated average group velocities of L(0,4) and L(0.6) are 4.1km/s and 3.2km/s, respectively, which coincide with the experimental results considering the errors so that the experimental results are verified.

4.2.2. Dynamic Verification. When the rotor rotates at 15Hz, the stress signals collected at the corresponding elements via FEM simulation are illustrated in Figure 11. The transmission signals obtained experimentally and numerically coincide with each other as well. L(0,4) and L(0,6) wave packages can be recognized clearly. The average calculated group velocities of L(0,4) and L(0,6) are 4.1km/s and 3.2km/s, respectively, which coincide with the group velocities acquired by the experiment when the rotor rotates at 15Hz and by the FEM simulation when the rotor is at rest. This result validates the experimental results when the rotor rotates at 15Hz. The conclusion that the longitudinal ultrasonic wave propagating

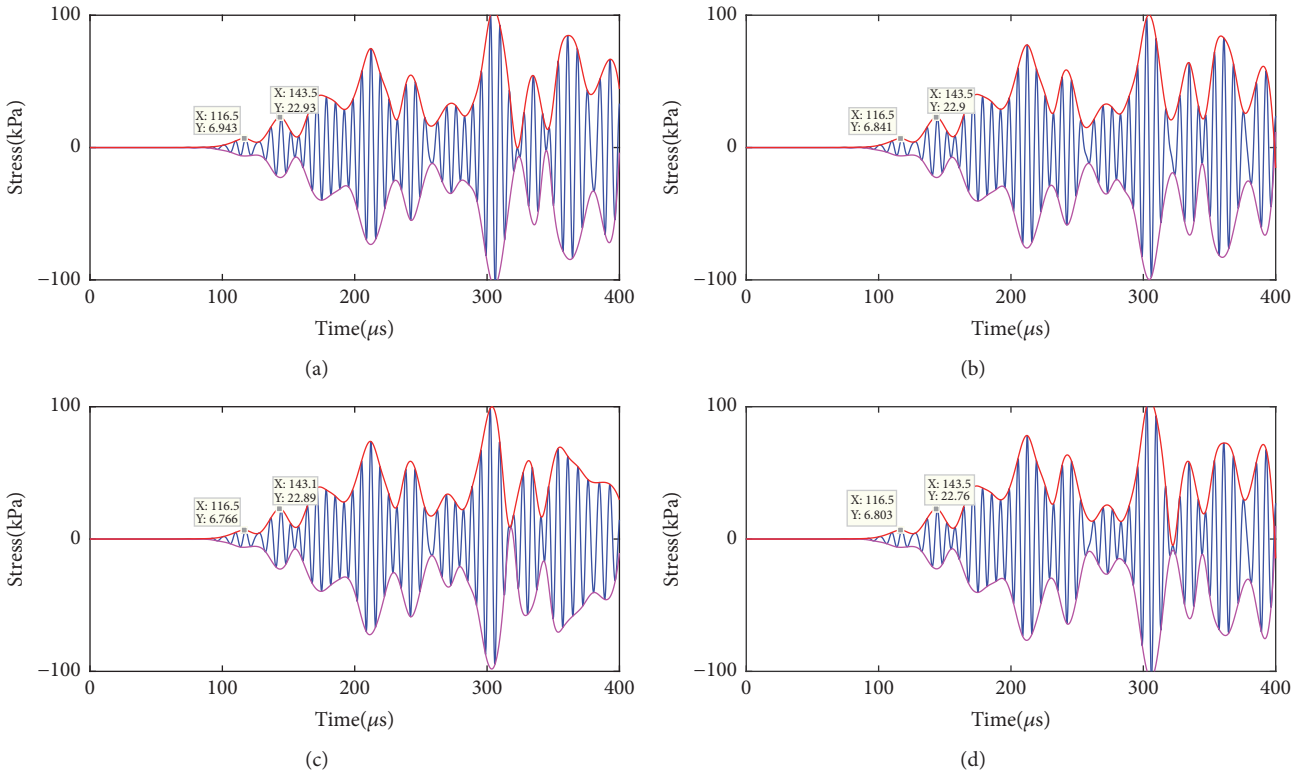

FIGURE 10: Collected signals of stress collection points (a) no. 1, (b) no. 2, (c) no. 3, and (d) no. 4 when the rotor is at rest.

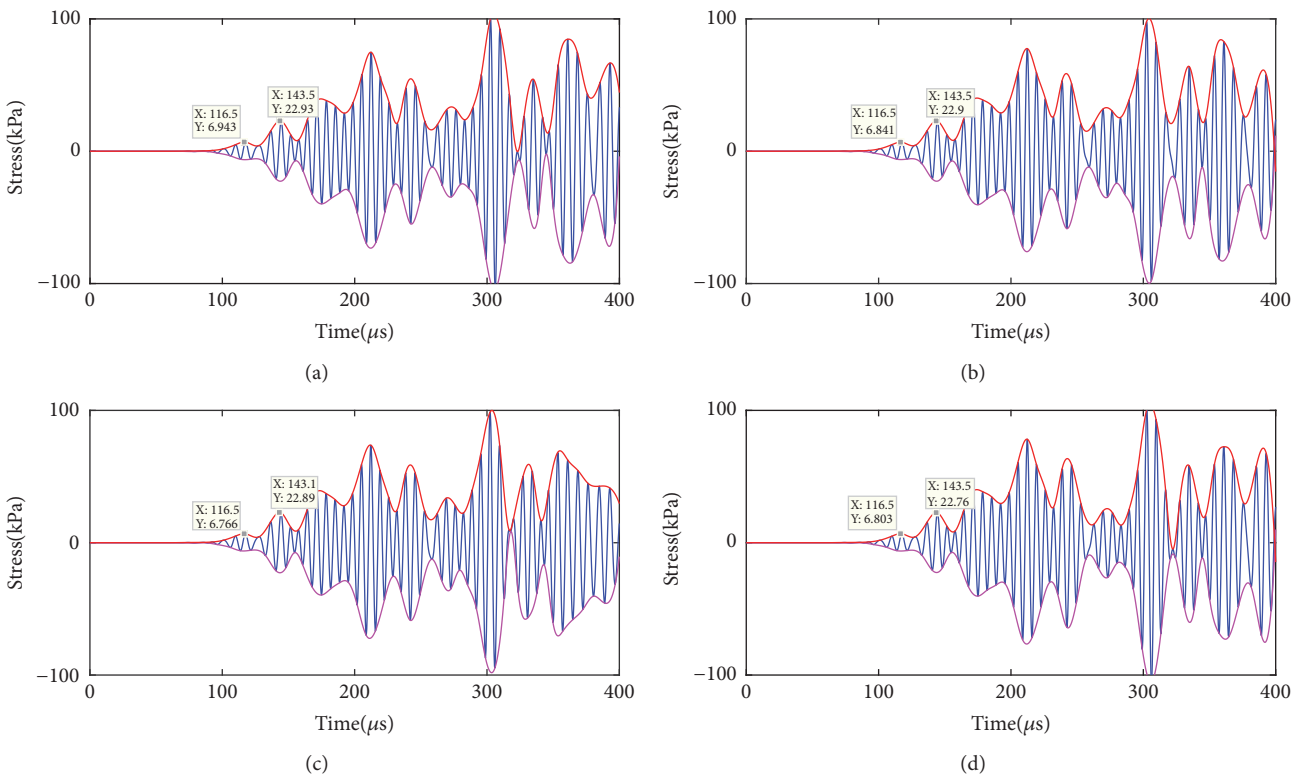

FIGURE 11: Collected signals of stress collection points (a) no. 1, (b) no. 2, (c) no. 3, and (d) no. 4 when the rotor rotates at 15Hz.

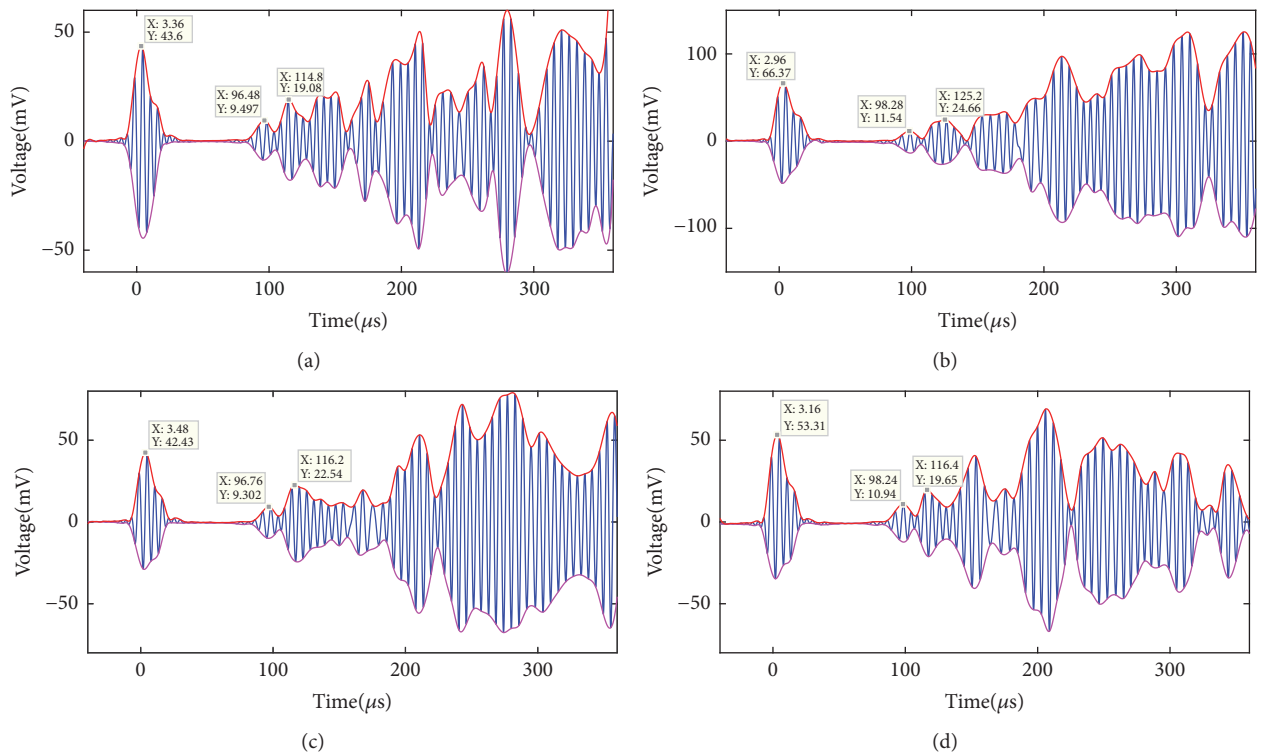

FIGURE 12: Collected signals of piezoelectric transducers after filtering (a) no. 1, (b) no. 2, (c) no. 3, and (d) no. 4 when the cracked rotor is at rest.

along the cylindrical shaft can hardly be interfered by the rotation proposed in paper [2] is also verified.

Therefore, the FEM simulations provide a support to the feasibility of the online SHM of a rotating shaft. The strategy for the online SHM will be established based on the above investigations.

5. Online Crack Detection of Rotating Shaft

5.1. Experimental Research. When encountering a crack, the ultrasonic wave will decompose into transmission wave, refraction wave, and reflection wave; therefore the existence of the crack should lead to a decline energy or amplitude of the collected signals. This phenomenon can be utilized for the online SHM for rotating machineries, especially the initial crack which can hardly be detected via vibration signal processing.

5.1.1. Static Research. The processed transmission wave signals collected by the piezoelectric transducers when the cracked rotor is at rest are illustrated in Figure 12. Comparing with the rotor without crack, the wave packages L(0,4) and L(0,6) can be intuitionally identified, and there is no sign of any mode conversion. In order to estimate the existence of the crack from the guided wave signals, define the amplitude ratio between L(0,4) wave package or L(0,6) wave package and the excitation signal as the relative amplitude. The relative amplitudes when the rotor is at rest with or without crack are listed in Table 1.

TABLE 1: Relative amplitudes of L(0,4) and L(0,6) without and with crack when the rotor is at rest.

	Without crack		With crack	
	L(0,4)	L(0,6)	L(0,4)	L(0,6)
1	0.207	0.402	0.218	0.438
2	0.212	0.433	0.174	0.372
3	0.195	0.478	0.219	0.531
4	0.234	0.439	0.205	0.369

It can be summarized from the relative amplitudes table that the 2nd transmission path leads to a declining relative amplitudes of L(0,4) and L(0,6), which is on account of the reflection wave. The relative amplitudes on the 4th transmission path, which is symmetric to the 2nd transmission path, decline as well, but with a less descending range than the 2nd transmission path. However, the relative amplitudes of L(0,4) and L(0,6) along the 1st and the 3rd transmission path ascend due to the refraction wave produced by the manufactured crack.

5.1.2. Dynamic Research. The processed transmission wave signals collected by the piezoelectric transducers when the cracked rotor rotates at 900rpm, i.e., 15Hz, are illustrated in Figure 13. Comparing with the rotor without crack, there is no mode conversion and the wave packages of L(0,4) and L(0,6) can be obviously identified. The calculated relative amplitudes are listed in Table 2.

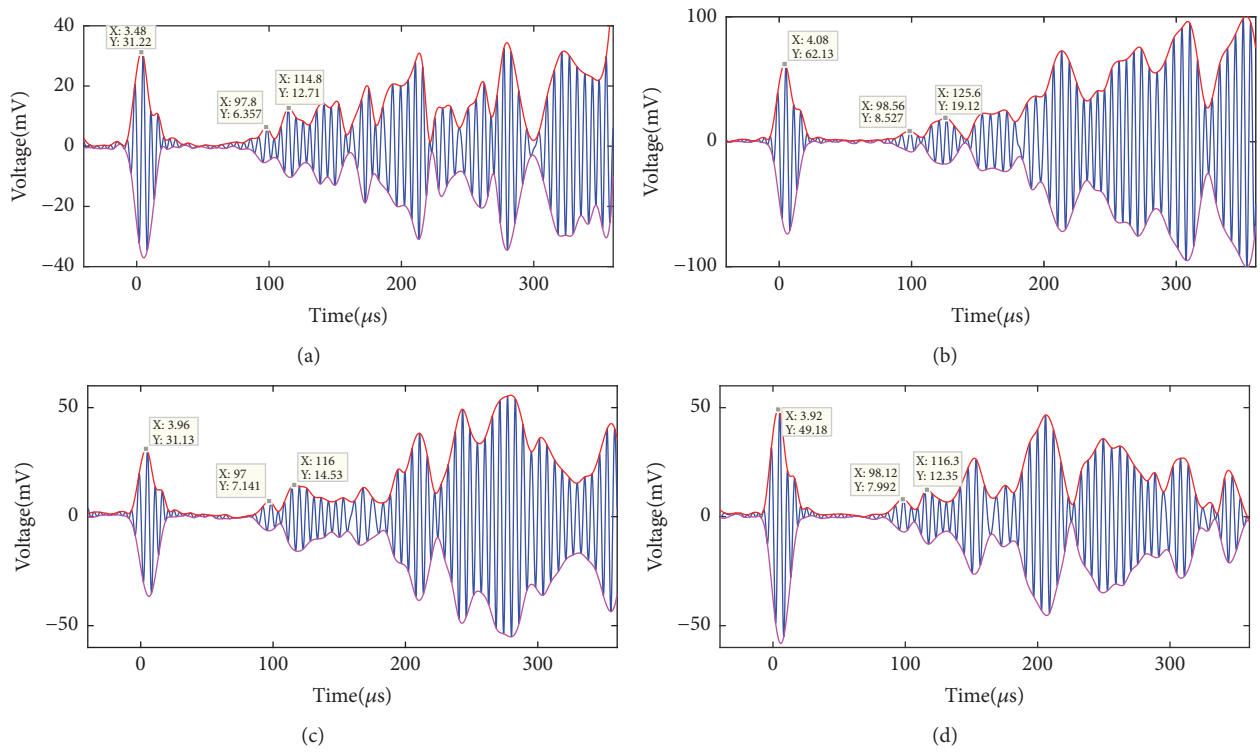

Figure 13: Collected signals of piezoelectric transducers after filtering (a) no. 1, (b) no. 2, (c) no. 3, and (d) no. 4 when the cracked rotor rotates at 15Hz.

Table 2: Relative amplitudes of L(0,4) and L(0,6) without and with crack when the rotor rotates at 15Hz.

	Without crack		With crack	
	L(0,4)	L(0,6)	L(0,4)	L(0,6)
1	0.207	0.429	0.204	0.407
2	0.198	0.408	0.137	0.308
3	0.151	0.330	0.229	0.467
4	0.169	0.243	0.163	0.251

It can be concluded from the table that the relative amplitudes of L(0,4) and L(0,6) along the 2nd transmission path both decline when the rotor is rotating at 15Hz. The amplitude of L(0,4) and L(0,6) along the 4th transmission path also declines but with a relatively smaller range. Different from the static research, the relative amplitudes of L(0,4) and L(0,6) along the 1st transmission path descend, but the relative amplitudes along the 3rd transmission path ascend. In this phenomenon an experimental error should be verified by the following FEM numerical simulation.

5.2. Numerical Verification

5.2.1. Static Verification. The stress signals collected at the corresponding elements via FEM simulation when the rotor is at rest are illustrated in Figure 14. The ultrasonic guided waves coincide with the signal obtained from the experiment, so that the experimental results of the rotor at rest are verified. Table 3 lists the amplitudes of L(0,4) and L(0,6) when the rotor is at rest with or without crack. It can be summarized that the amplitudes of L(0,4) and L(0,6) decline along the 2nd transmission path, and the amplitudes of L(0,4) and L(0,6) have a less decline along the 4th transmission path due to the reflection wave. The amplitudes of L(0,4) and L(0,6) along both the 1st and the 3rd transmission path ascend because of the fraction wave.

The numerical simulation verifies the experimental research when the cracked rotor is at rest. The strategy dealing with the SHM of the rotor at rest can be concluded that when the 4-piece excitation transducers and collection transducers are arranged axial symmetrically, comparing with the rotor without crack, the amplitudes of L(0,4) and L(0,6) along the transmission path where crack occurs descend, so with the amplitudes of L(0,4) and L(0,6) along the symmetric transmission path but with a less range, the amplitudes of L(0,4) and L(0,6) along the other transmission paths ascend.

5.2.2. Dynamic Verification. The stress signals collected at the corresponding elements via FEM simulation when the rotor rotates at 15Hz are illustrated in Figure 15. The ultrasonic guided waves coincide with the experimental results and the wave packages L(0,4) and L(0,6) can be identified intuitionally, which verifies the experimental research. Table 4 lists the amplitudes of L(0,4) and L(0,6) when the rotor rotates at 15Hz with or without crack. It can be summarized from the table that, due to the reflection wave, the amplitudes of L(0,4) and L(0,6) along the 2nd transmission path descend.

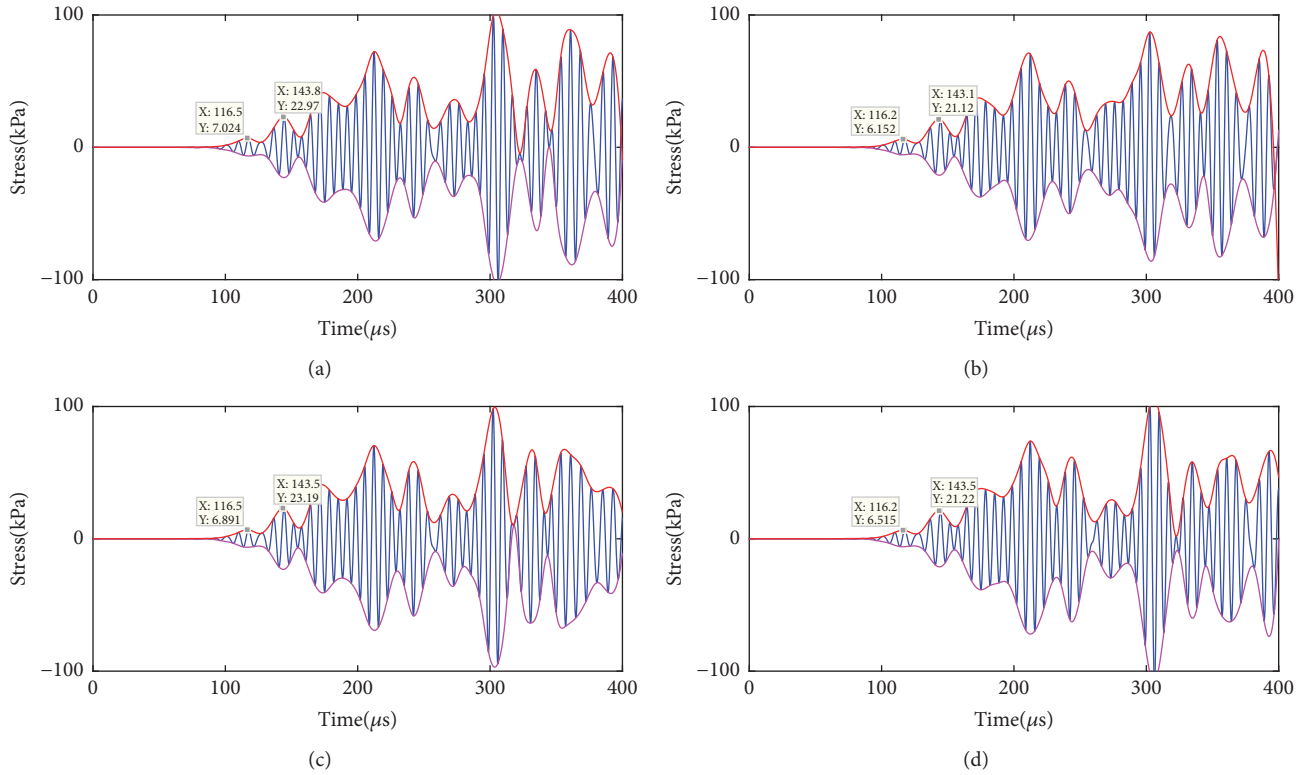

Figure 14: Collected signals of stress collection points (a) no. 1, (b) no. 2, (c) no. 3, and (d) no. 4 when the rotor is at rest.

Table 3: Amplitudes of L(0,4) and L(0,6) without and with crack when the rotor is at rest.

kPa	Without crack		With crack	
	L(0,4)	L(0,6)	L(0,4)	L(0,6)
1	6.943	22.93	7.024	22.97
2	6.841	22.90	6.152	21.12
3	6.766	22.89	6.891	23.19
4	6.803	22.76	6.515	21.22

The amplitudes of L(0,4) and L(0,6) along the 4th transmission path have a relatively less decline. It should be noted that, in this numerical simulation, both the amplitudes of L(0,4) and L(0,6) along the 1st and 3rd transmission path ascend.

The numerical simulation partially verifies the experimental results. The amplitudes of L(0,4) and L(0,6) along the 1st transmission path descend in the experiment but ascend in the numerical simulation. This phenomenon can be categorized into experimental error and the reason should be further investigated. Therefore, the strategy dealing with the online SHM of the rotating shaft can be concluded that when the 4-piece excitation transducers and collection transducers are arranged axial symmetrically, comparing with the rotor without crack, the amplitudes of L(0,4) and L(0,6) along the transmission path where crack occurs descend, and so with the amplitudes of L(0,4) and L(0,6) along the symmetric transmission path but with a less range, the amplitudes of L(0,4) and L(0,6) along the other transmission paths ascend. This strategy is the same with the strategy when the rotor is at rest, which is a justification on the conclusion that the longitudinal ultrasonic wave propagating along the cylindrical shaft can hardly be interfered by the rotation as well.

6. Conclusion

Based on the above investigations, the online SHM strategy for rotating shafts can be concluded as follows. The excitation signal should be firstly decided via the dispersion curves of the rotating cylindrical shaft, which is the same with the cylindrical shaft at rest. The excited modes, especially the longitudinal modes which carry majority of the energy, should be as few as possible in order to avoid the overlapping between wave packets. The target modes should be faster than other modes so that the wave packets can be clearly identified. Four-piece excitation transducers and corresponding collection transducers are arranged axial symmetrically along the rotor. The electric signals between the transducers and the devices are transmitted through a slip ring. Comparing with the rotor without crack, the amplitudes of the wave packages along the transmission path where crack occurs descend, so with the amplitudes of the wave packages along the symmetric transmission path but with a less range, the amplitudes of the wave packages along the other transmission paths ascend. This online SHM strategy has been verified via experimental research and numerical simulation; however,

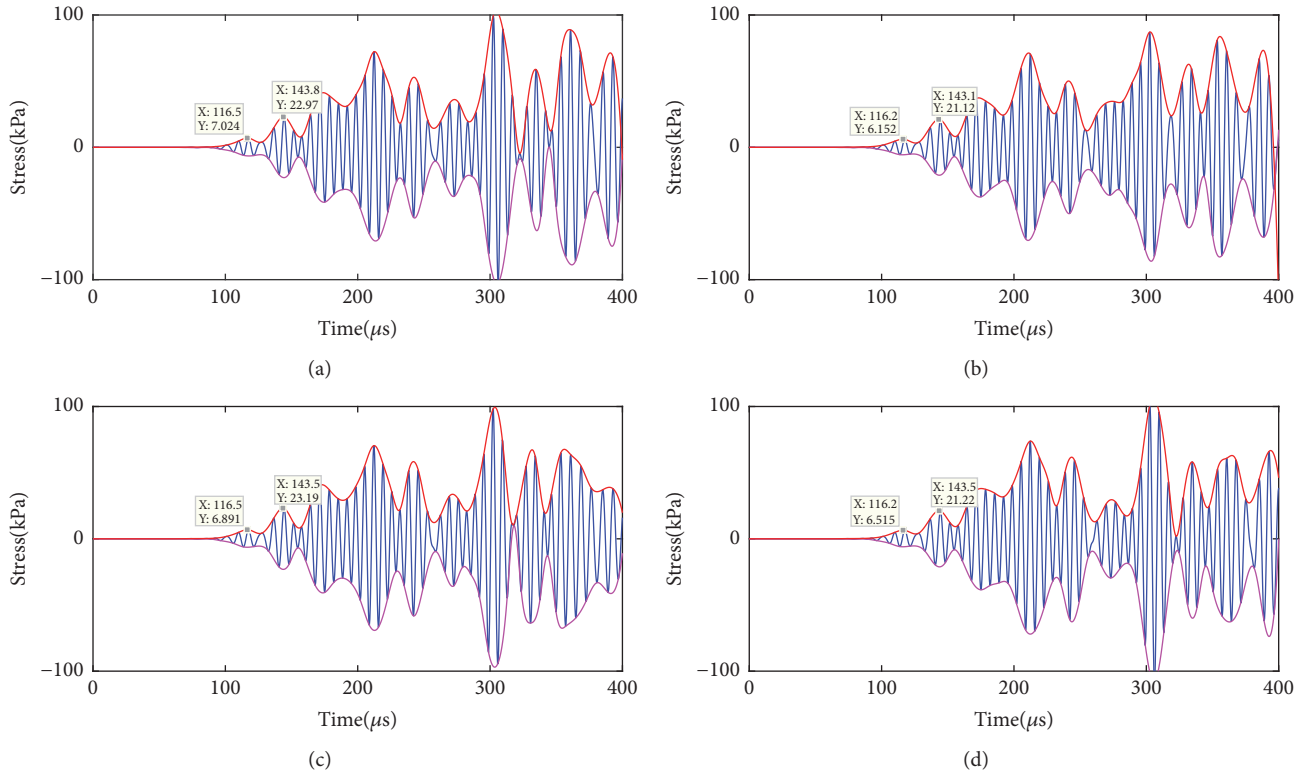

Figure 15: Collected signals of stress collection points (a) no. 1, (b) no. 2, (c) no. 3, and (d) no. 4 when the rotor rotates at 15Hz.

Table 4: Amplitudes of L(0,4) and L(0,6) without and with crack when the rotor rotates at 15Hz.

kPa	Without crack		With crack	
	L(0,4)	L(0,6)	L(0,4)	L(0,6)
1	6.943	22.93	7.024	22.97
2	6.841	22.90	6.152	21.12
3	6.766	22.89	6.891	23.19
4	6.803	22.76	6.515	21.22

there is still some insufficiency should be improved, which would be implemented in subsequent researches.

Data Availability

The data used to support the findings of this study are available from the corresponding author upon request.

Conflicts of Interest

The authors declare that they have no conflicts of interest.

Acknowledgments

The authors are grateful for the supports received from Shanghai Sailing Program (Grant no. 17YF1419300), the Science Fund for Creative Research Groups of the National Natural Science Foundation of China (Grant no. 51421092), and the National Basic Research Program of China (973 Program, Grant no. 2011CB706502).

References

[1] Y. Ishida, "Cracked rotors: industrial machine case histories and nonlinear effects shown by simple Jeffcott rotor," *Mechanical Systems and Signal Processing*, vol. 22, no. 4, pp. 805–817, 2008.

[2] M. Li, H. Bai, X. Wang, H. Li, F. Li, and G. Meng, "Dynamic Saint-Venant principle for rotor system with undetectable initial crack," *Archive of Applied Mechanics*, vol. 86, no. 11, pp. 1841–1851, 2016.

[3] J. J. Ditria, "Utilization of guided elastic waves for the characterization of circumferential cracks in hollow cylinders," *The Journal of the Acoustical Society of America*, vol. 96, no. 6, pp. 3769–3775, 1994.

[4] W. Zhu, J. L. Rose, J. N. Barshinger, and V. S. Agarwala, "Ultrasonic guided wave NDT for hidden corrosion detection," *Research in Nondestructive Evaluation*, vol. 10, no. 4, pp. 205–225, 1998.

[5] M. J. S. Lowe, D. N. Alleyne, and P. Cawley, "Defect detection in pipes using guided waves," *Ultrasonics*, vol. 36, no. 1–5, pp. 147–154, 1998.

[6] J. Qu, Y. Berthelot, and L. Jacobs, "Crack detection in thick annular components using ultrasonic guided waves," *Proceedings of the Institution of Mechanical Engineers, Part C: Journal of Mechanical Engineering Science*, vol. 214, no. 9, pp. 1163–1171, 2000.

[7] D. Tuzzeo and F. L. di Scalea, "Noncontact air-coupled guided wave ultrasonics for detection of thinning defects in aluminum

plates," *Research in Nondestructive Evaluation*, vol. 13, no. 2, pp. 61–77, 2001.

[8] F. L. di Scalea, P. Rizzo, and F. Seible, "Stress measurement and defect detection in steel strands by guided stress waves," *Journal of Materials in Civil Engineering*, vol. 15, no. 3, pp. 219–227, 2003.

[9] J. N. Barshinger and J. L. Rose, "Guided wave propagation in an elastic hollow cylinder coated with a viscoelastic material," *IEEE Transactions on Ultrasonics, Ferroelectrics and Frequency Control*, vol. 51, no. 11, pp. 1547–1556, 2004.

[10] I. Bartoli, F. L. Di Scalea, M. Fateh, and E. Viola, "Modeling guided wave propagation with application to the long-range defect detection in railroad tracks," *NDT & E International*, vol. 38, no. 5, pp. 325–334, 2005.

[11] F. C. Li, H. Murayama, K. Kageyama, and T. Shirai, "Guided wave and damage detection in composite laminates using different fiber optic sensors," *Sensors*, vol. 9, no. 5, pp. 4005–4021, 2009.

[12] F. Song, G. L. Huang, and K. Hudson, "Guided wave propagation in honeycomb sandwich structures using a piezoelectric actuator/sensor system," *Smart Materials and Structures*, vol. 18, no. 12, 2009.

[13] X. Miao, D. Wang, L. Ye, Y. Lu, F. Li, and G. Meng, "Identification of dual notches based on time-reversal lamb waves and a damage diagnostic imaging algorithm," *Journal of Intelligent Material Systems and Structures*, vol. 22, no. 17, pp. 1983–1992, 2011.

[14] F. Li, Z. Liu, X. Sun, H. Li, and G. Meng, "Propagation of guided waves in pressure vessel," *Wave Motion*, vol. 52, pp. 216–228, 2015.

[15] S. W. Han, H. C. Lee, and Y. Y. Kim, "Noncontact damage detection of a rotating shaft using the magnetostrictive effect," *Journal of Nondestructive Evaluation*, vol. 22, no. 4, pp. 141–151, 2003.

[16] S. H. Cho, S. W. Han, C. I. Park, and Y. Y. Kim, "Noncontact torsional wave transduction in a rotating shaft using oblique magnetostrictive strips," *Journal of Applied Physics*, vol. 100, no. 10, 2006.

[17] Y. Kim and Y. Y. Kim, "A novel Terfenol-D transducer for guided-wave inspection of a rotating shaft," *Sensors and Actuators A: Physical*, vol. 133, no. 2, pp. 447–456, 2007.

[18] X. Wang, J. Zou, F. Wang, and R. Li, "Longitudinal ultrasonic guided waves for monitoring the minor crack of rotating shaft with Galfenol transducer," *Sensors & Transducers Journal*, vol. 159, no. 11, pp. 450–456, 2013.

[19] J.-L. Auriault, "Body wave propagation in rotating elastic media," *Mechanics Research Communications*, vol. 31, no. 1, pp. 21–27, 2004.

[20] J. Sharma and D. Grover, "Body wave propagation in rotating thermoelastic media," *Mechanics Research Communications*, vol. 36, no. 6, pp. 715–721, 2009.

[21] M. Onoe, H. D. McNiven, and R. D. Mindlin, "Dispersion of axially symmetric waves in elastic rods," *Journal of Applied Mechanics*, vol. 29, pp. 729–734, 1962.

[22] K. F. Graff, *Wave Motion in Elastic Solids*, Oxford University Press, London, UK, 1975.

[23] Y.-H. Pao and R. D. Mindlin, "Dispersion of flexural waves in an elastic, circular cylinder," *Journal of Applied Mechanics*, vol. 27, pp. 513–520, 1960.

[24] Y.-H. Pao, "The dispersion of flexural waves in an elastic, circular cylinder—part 2," *Journal of Applied Mechanics*, vol. 29, pp. 61–64, 1962.

[25] M. Li, X. Liu, R. Zhu et al., "Rotor dynamics behavior of tilting pad bearing supported turbo-expander considering temperature gradient," *Journal of Computational and Nonlinear Dynamics*, vol. 11, no. 2, 2016.

[26] K. Sun, G. Meng, F. Li, L. Ye, and Y. Lu, "Damage detection in thick steel beam using lamb waves," in *Proceedings of the ASME 2008 Conference on Smart Materials, Adaptive Structures and Intelligent Systems*, pp. 201–207, Ellicott City, MD, USA, 2008.

[27] H. Peng, G. Meng, and F. Li, "Modeling of wave propagation in plate structures using three-dimensional spectral element method for damage detection," *Journal of Sound and Vibration*, vol. 320, no. 4-5, pp. 942–954, 2009.